High-dimensional quantum dynamical study of the dissociation of H_2 on Pd(110)

Arezoo Dianat and Axel Groß
Physik-Department T30, Technische Universität München, D-85747 Garching, Germany
(Dated: October 31, 2003)

We report the first six-dimensional quantum dynamical study of the dissociative adsorption of H_2 on a (110) surface. We have performed quantum coupled-channel calculations for the system H_2/Pd(110) based on a potential energy surface (PES) that was derived from *ab initio* electronic structure calculations. In particular, we have focused on the effects of the corrugation and anisotropy of the PES on the H_2 dissociation probability. Our results agree well with the available experimental data for the sticking probability as a function of the initial kinetic energy and the angle of incidence. Because of the coupling between the anisotropy and corrugation of the potential energy surface our calculations predict an unusual rotational heating and a rather small rotational alignment in desorption.

I. INTRODUCTION

The dynamics of the dissociative adsorption and associative desorption of H_2 on metal surfaces has served as a model system for the study of simple reactions at surfaces in the last years, both experimentally[1–12] as well as theoretically[13–30]. In particular, the influence of the kinetic energy, the vibrational and rotational motion and the angle of incidence on the adsorption and desorption dynamics has been studied in detail. Based on a close interaction between experiment and theory, these investigations have elucidated a number of fundamental microscopic reaction mechanisms that are applicable to the dissociation dynamics of molecules in general.

As far as the theoretical description is concerned, quantum dynamical studies in which all six degrees of freedom of the H_2 molecule are explicitly included can nowadays almost routinely be performed[14–16,26,29,31]. These studies have all considered the low-index (100) and (111) surfaces since their high symmetry allows a considerable reduction of the computational effort by using symmetry-adapted wave functions[15,32,33].

In this paper, we report the first six-dimensional quantum dynamical study of H_2 dissociation on a (110) surface, namely for the system H_2/Pd(110). The potential energy surface (PES) used in our study has been derived from first-principles electronic structure calculations based on density functional theory (DFT) within the generalized gradient approximation[34], and the dynamical calculations have been carried out employing a computationally very efficient coupled-channel scheme[35,36].

We have in particular focused on the effects of the corrugation and anisotropy of the PES on the H_2 dissociation probability. The (110) surface exhibits a rather open structure with troughs running along the $[1\bar{1}0]$ direction. Our results agree well with the available experimental data for the sticking probability as a function of the initial kinetic energy and the angle of incidence. We have further analysed the influence of the initial rotational state characterized by the rotational quantum numbers j and m. Molecules rotating in the so-called cartwheel fashion $m = 0$ with their molecular axis preferentially oriented perpenducular to the surface have a smaller sticking probability than non-rotating molecules. This is a well-known result[14,17,19]. However, we find a surprinsingly large rotational enhancement of the dissociation probability if the preferential orientation of the molecular axis is slightly further off from the perpendicular orientation, i.e., for $m > 0$. We attribute this to the strong coupling between the corrugation and anisotropy of the potential energy surface. Based on these findings, we predict an unusual rotational heating and a rather small rotational alignment in desorption. For non-normal incidence, we find a strong deviation from normal-energy scaling which also depends on the azimuthal angle of incidence.

This paper is structured as follows. After this introduction we first describe the construction of the potential energy surface and the computational details of the quantum dynamical calculations. Then we discuss the results of our calculations with respect to the influence of the kinetic energy, rotational state and angle of incidence on the dissociation dynamics. The paper ends with some concluding remarks.

II. THEORETICAL METHODS

In order to perform the quantum dynamical simulations, we need a continuous analytical form of the potential energy surface. Consequently, the first step is the parametrization of the *ab initio* PES as a function of the six coordinates of the H_2 molecule using a suitable analytical form. These six coordinates are the center-of-mass position (X, Y, Z), the interatomic distance r and the polar and azimuthal orientation of the molecular axis θ and ϕ, respectively. The metal substrate is usually kept fixed in the quantum dynamical simulations. This approximation is justified by the large mass mismatch between hydrogen and the metal atoms which makes any energy transfer and substrate rearrangement during the collision time rather improbable.

The PES of H_2 interacting with surfaces is usually analysed in terms of so-called elbow potentials which correspond to two-dimensional cuts through the six-dimensional PES as a function of the molecular distance from the surface Z and the interatomic H-H distance r for fixed lateral center-of-mass coordinates and molecular orientation. In the DFT calculations, such elbow plots are determined at high-symmetry points of the surface unit cell.

In Fig. 1, two elbow plots are shown which are in fact derived from the analytical fit to the *ab initio* PES[34]. In the insets of Fig. 1, the coordinate axes of the surface unit cell are defined. In the following, we will denote by [10] or x the [1$\bar{1}$0] direction and by [01] or y the [001] direction. In a quantum coupled scheme, the wave function as a function of the coordinates perpendicular to a chosen reaction path coordinate is expanded in a set of suitable eigenfunctions. Usually, one chooses the curvelinear coordinate along one minimum energy path of an elbow plot as the reaction path coordinate s; the coordinate perpendicular to the reaction path is denoted by ρ. Hence the six-dimensional potential energy surface in reaction path coordinates is defined by $V(X, Y, s, \rho, \theta, \phi)$. In the parametrization employed in this work we break up the PES in several contributions due to the corrugation, the anisotropy and the intramolecular vibration

$$V(X, Y, s, \rho, \theta, \phi) = V^{corr} + V^{rot} + V^{vib} \qquad (1)$$

By anisotropy we mean the explicit dependence of the potential on the molecular orientation. However, it is important to note that for a molecule interacting with a corrugated surface, the anisotropy and corrugation are not independent: the anisotropy strongly varies as a function of the lateral position of the molecule. Hence anisotropy and corrugation are intimately linked.

The explicit functional form we have chosen is given by

$$\begin{aligned} V^{corr} &= V_0^c(s) + V_1^c(s)\cos G_X X + V_2^c(s)\cos G_Y Y \\ &\quad + V_3^c(s)\cos G_X X \cos G_Y Y \end{aligned} \qquad (2)$$

$$\begin{aligned} V^{rot} &= V_0^r(s)\cos^2\theta + [V_1^r(s)\cos G_X X + V_2^r(s)\cos G_Y Y \\ &\quad + V_3^r(s)\cos G_X X \cos G_Y Y]\sin^2\theta\cos(2\phi) \end{aligned} \qquad (3)$$

$$V^{vib} = \frac{\mu}{2}\omega^2(s)[\rho - \Delta\rho(s, X, Y)]^2 \qquad (4)$$

This PES is constructed by considering two polar orientations of the molecular axis, parallel (θ= 90°) and perpendicular (θ= 0°) to the surface. For the parallel geometry, we have used the published H_2/Pd(110) elbow plots obtained in DFT calculations by Ledentu *et al.*[34]. The direction corresponding to ϕ= 0° is associated with the molecular axis of H_2 aligned along the [10] or x direction. Out of the nine published elbow plots we have used six to adjust the parameters in our interpolation scheme. The remaining three elbow plots have served as test examples. Unfortunately, no *ab initio* data for the perpendicular H_2 orientation on Pd(110) was available. Assuming that the polar anisotropy of the H_2/Pd PES does not vary significantly between different low-index Pd surfaces, we have used the laterally independent polar anisotropy calculated for the H_2/Pd(100) system[15,37].

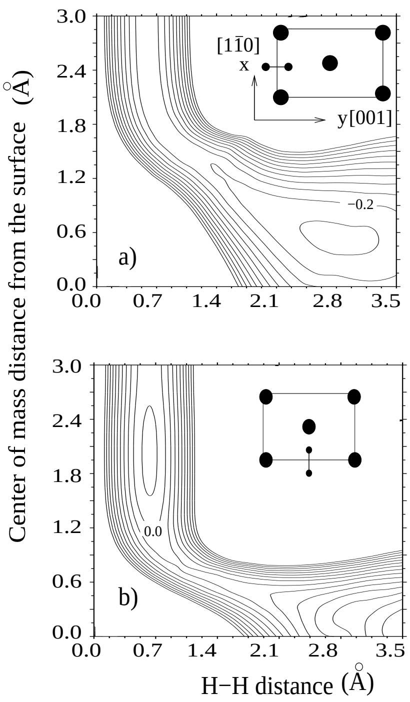

FIG. 1: Elbow potentials of H_2 at the short bridge (a) and the long bridge (b) position of Pd(110) according to the analytical interpolation of the *ab initio* results[34]. The coordinates are the H_2 center of mass distance from the surface Z and the H-H interatomic distance r. The molecular orientation is parallel to the surface and perpendicular to the corresponding bridge, as indicated in the insets. The level spacing of the contour lines is 0.2 eV.

The functions of the reaction path coordinate s appearing in Eqs. (1)–(4) are given by suitable analytical expressions mainly consisting of tanh and $\cosh^{-2}$ terms, as for example also used in Ref. 17. In the fit, we have mainly tried to obtain an accurate representation of the PES close to the transition states since these regions are crucial for the dissociation dynamics. As far as the transition state energies of the adsorption paths determined by Ledentu *et al.*[34] are concerned, the mean difference between the *ab inition* results and the interpolation is below 50 meV. Generally, the deviation is about 100 meV on the average.

In Fig. 1, two parametrized elbow potentials are plotted for the H_2 molecule above the so-called short-bridge and long-bridge position, respectively, with its molecular axis parallel to the surface and perpendicular to the bridge axes. Fig. 1a corresponds to the most favorable reaction route along which H_2 molecules can spontaneously dissociate. It smoothly leads from the molecule in the gas phase to the dissociated atoms on the surface. This contour plot corresponds to Fig. 2b of Ref. 34. Note that the regions of the elbow plot for H-H distances above approximately 2.0 Å which are not crucial for the dissociation dynamics have been fitted with less accuracy. At the long-bridge position (Fig. 1b), the dissociation is no longer non-activated, and there is a shallow minimum before the barrier which is, however, only about 100 meV high. Furthermore, the minimum energy path bends much more sharply. It is important to note that the PES of H_2 on Pd(110) consists of a combination of non-activated and activated paths to dissociative adsorption.

It should also be emphasized here that using a parametrization such as Eqs. (1)–(4) which is adjusted to *ab initio* calculations at high-symmetry points represents an assumption about the form of the PES at low-symmetry configurations which does not necessarily be correct. That is to say that even if the *ab initio* PES is accurately reproduced by the parametrization at high-symmetry points, it might not be well-reproduced in the interpolated regions. However, in the absence of *ab initio* calculations for low-symmetry configurations it is not possible to judge the reliability of this interpolation.

Using the parametrization of the *ab initio* PES, the time-independent Schrödinger equation for the two hydrogen nuclei moving on the six-dimensional PES has been solved by coupled-channel calculations using the concept of the *local reflection matrix* (LORE) and the *inverese local transmission matrix* (INTRA)[35,36]. As usual, the H_2 dissociation probability is identified with the transmission probability to enter the dissociation channel (large s) from the gas phase. The quantum mechanical scattering solutions are expressed as a superposition of plane waves for the lateral motion of the H_2 center of mass, spherical harmonics for the rotational motion and harmonic oscillator eigenfunctions for the vibrational motion perpendicular to the reaction path:

$$\Psi(X,Y,s,\rho,\theta,\phi) = \sum_{\vec{G}_{\|}lmi} \Phi_{\vec{G}_{\|}lmi}(s) e^{i(\vec{G}_{\|}+\vec{k}_{\|})\cdot\vec{R}_{\|}} \; Y_{lm}(\theta,\phi)\chi_i(\rho) \ , \quad (5)$$

where $\vec{R}_{\|}$ is the two-dimensional vector (X,Y) describing the lateral coordinates of the H_2 center of mass, and $\vec{G}_{\|}$ are vectors of the two-dimensional reciprocal lattice of the surface. Using mass-scaled reaction path coordinates in the Zr plane, we employ the six-dimensional Hamiltonian given by[15]

$$\begin{aligned} H_{6D} \; = \; & -\frac{\hbar^2}{2\mu}\left(\eta^{-1}\frac{\partial}{\partial s}\eta^{-1}\frac{\partial}{\partial s} + \eta^{-1}\frac{\partial}{\partial \rho}\eta\frac{\partial}{\partial \rho} + \frac{\vec{L}^2}{r_e^2}\right) \\ & -\frac{\hbar^2}{2M}\left(\frac{\partial^2}{\partial X^2}+\frac{\partial^2}{\partial Y^2}\right) + \; V(X,Y,s,\rho,\theta,\phi) \quad (6) \end{aligned}$$

Here, μ is the reduced mass of the H_2 molecule, M is its total mass, $\vec{L}$ is the angular momentum operator, r_e the H_2 minimum energy bond length, and the coupling parameter η is defined by

$$\eta \; = \; 1 \; - \kappa(s)\; \rho \ , \quad (7)$$

where $\kappa(s)$ is the curvature of the lowest energy reaction path (see Fig. 1a). The potential is expressed as matrix elements along the reaction path coordinate $V_{\vec{G}_{\|}lmi,\vec{G}'_{\|}l'm'i'}(s)$ with respect to the basis function defined in Eq. (5). The basis set used in the coupled-channel algorithm included rotational quantum numbers up to j_{max}=8, vibrational quantum number up to ν_{max}=2 and maximum parallel momentum $p_{max}=10\hbar G$ with $G = \min(G_X, G_Y) = \min(2\pi/a_X, 2\pi/a_Y) = 2\pi/a_Y$, where a_X and a_Y are the lattice constants of the surface unit cell of the (110) surface along the [10] and [01] directions, respectively.

The convergence of the results as a function of the size of the basis set has been carefully checked. Since the vibration corresponds to the fastest time-scale in the H_2 dynamics, its motion is effectively decoupled from the motion of the remaining degrees of freedom. Therefore, five-dimensional vibrationally adiabatic calculations give results very similar to full six-dimensional calculations[38]. Because of the greatly reduced computational effort, the majority of results presented below have been obtained in 5D vibrationally adiabatic calculations. However, we have carefully checked whether there is a significant deviation between 5D and 6D results.

III. RESULTS AND DISCUSSION

In Fig. 2, we have plotted the calculated sticking probability of H_2 impinging on Pd(110) under normal incidence as a function of the kinetic energy for different initial rotational states. In Fig. 2b, results of a molecular beam experiment are included. It is obvious that the observed non-monotonous behavior of the sticking probability as a function of the kinetic energy is well-reproduced for initially non-rotating molecules ($j = 0$) in the calculations. It is now well accepted that the initial decrease of the H_2 sticking probability in non-activated dissociation systems with increasing energy is a consequence of the suppression of the steering effect[14,15,27,28,40]: At low kinetic energies, the slow molecules can be very efficiently steered to nonactivated pathways towards dissociative adsorption by the attractive forces of the potential. This mechanism becomes less effective at higher translational energy leading to smaller dissociation probabilities. A more detailed analysis of the adsorption dynamics yields that a low energies many incoming molecules are trapped in a transient state due to dynamic trapping[27,28]: they do not directly dissociate but transfer energy from the translation perpendicular to the surface into internal degrees of freedom and motion parallel to the surface so that they cannot escape back to the vacuum. Eventually most of the dynamically trapped molecules dissociate.

Just recently, the dissociative adsorption of H_2/Pd(110) for normal incidence has been studied

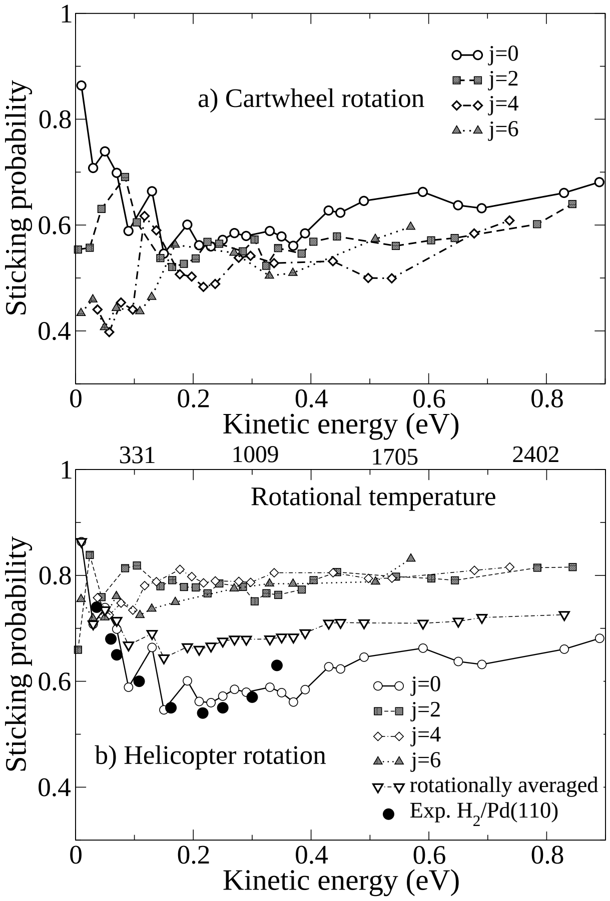

FIG. 2: Calculated sticking probability of H_2 for a range of initial rotational states j as a function of kinetic energy under normal incidence. a) Molecules initially rotating in the cartwheel fashion $m = 0$, b) molecules initially rotating in the helicopter fashion $m = j$. The rotationally averaged results have been determined by averaging over rotational quantum numbers according to a Boltzmann distribution with a rotational temperature $T_{\rm rot} = 0.8\,T_N$, where T_N is the nozzle temperature. The corresponding rotational temperatures are indicated above the figure. In addition, the experimental results of a molecular beam experiment are included[39].

by classical and quasiclassical molecular dynamics simulations[30]. In these calculations, a PES has been employed that was adjusted to DFT calculations in a corrugation-reducing scheme[41]. This study mainly focused on the role of dynamic trapping. The calculated sticking probabilities are in good agreement to the ones determined by us, regarding the different methods used in both studies.

In molecular beam experiments, supersonic beams of molecules are directed at the surface of interest. These beams are formed by the rapid expansion of a gas flowing through a nozzle which leads to translational energy distributions that are considerably narrower than those of thermal beams[5]. The mean translational energy is primarily controlled by chosing the temperature T_N of the nozzle through which the molecule emerge. This has the unwanted side-effect of changing the populations of the initial rovibrational states, which are usually given by a Boltzmann distribution according to some effective temperature. Thus many plots of S(E) are actually S(T_N) curves. These are only the same when vibration and rotation have no influence on the dissociation. However, as we see in Fig. 2, the dissociation probability strongly depends on the rotational state.

Figure 2a shows the sticking probability for molecules rotating in the cartwheel fashion with $m = 0$. In these rotational states, the molecules have a high probability to hit the surface in an upright orientation in which they cannot dissociate. In addition, the dissociation probability is further reduced for molecules that are more rapidly rotating (higher j), in particular a low kinetic energies. Rapidly rotating molecules will rotate out of a favorable configuration for dissociation during the interaction with the surface. This rotational hindering[17,19] becomes less pronounced at higher kinetic energies where the impinging molecules are rather fast.

The rotational hindering can in fact be counterbalanced by orientational or steric effects. If the molecules are rotating in the so-called helicopter fashion with $m = j$, then the rotational axis of the H_2 molecule is preferentially oriented perpendicular to the surface which means that the molecular axis is preferentially parallel to the surface. This orientation is favorable for dissociation. As Fig. 2b shows, additional helicopter rotation indeed leads to an enhanced sticking probability, which has also been found at other surfaces[14,17]. Interestingly, the rotational enhancement of the sticking probability for helicopter molecules seems to be independent of the particular rotational quantum number j. We note that for higher rotational quantum numbers there is also a rotationally adiabatic effect in dissociative adsorption since the bond length $r_e(s)$ and thus the moment of inertia $I = \mu r_e^2(s)$ increases[17,19]. For rotationally adiabatic motion, the rotational energy

$$E_{rot}(j) = \frac{\hbar^2 j(j+1)}{2I} \quad (8)$$

in a particular rotational state decreases due to the rise in the moment of inertia I which leads to an effective energy transfer from rotation to translation. As Fig. 1 indicates, the minimum energy paths in the elbow plots of the PES exhibit a strong curvature. If there were no rotationally adiabatic effects, one would expect that the dissociation probability decreases monotonously with increasing j, in particular for molecules rotating in the cartwheel fashion[17]. Figure 2a shows that the rotational hindering does not rise any further for $j \geq 4$. This is an indication that bond length effects play a significant role in the dissociation dynamics[17,19]. In particular it means that the adiabatic energy transfer from rotations to translations contributes to the rotational effects in the system H_2/Pd(110).

In order to analyse the dependence of the sticking prob-

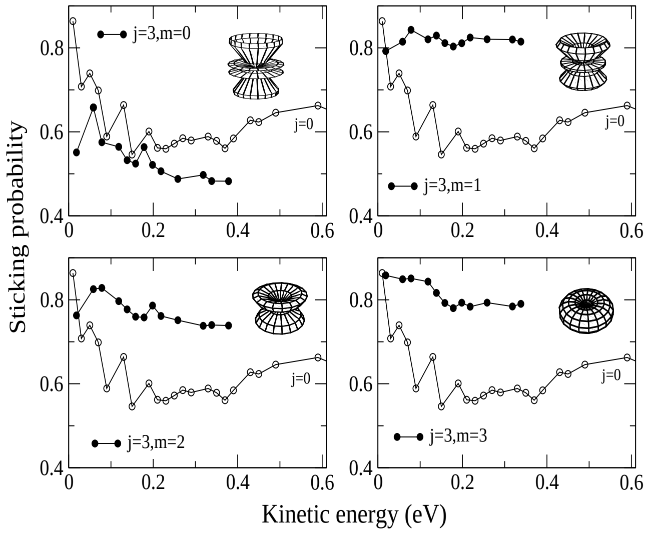

FIG. 3: Calculated sticking probability of H_2/Pd(110) as a function of kinetic energy for H_2 molecules initially in the $j = 3$ state for different azimuthal quantum numbers m. For the sake of comparison, the results for $j = 0$ are also included. The insets show the probability distibution of the corresponding $(j = 3, m)$ rotational state.

ability on the rotational state in more detail, we have plotted in Fig. 3 the calculated results for H_2 molecules initially in the $j = 3$ state as a function of the azimuthal quantum number m. For $(j = 3, m = 0)$, we find the expected rotational hindering for this cartwheel mode. However, interestingly enough we find for all states with $(j = 3, m > 0)$ a significant enhancement of the sticking probability. We have confirmed that this is indeed true not only for the $j = 3$ states, but also for the other j states. This strong enhancement represents a surprising results. As far as the rotational effects in the dissociation of H_2 at the more densely packed (111) and (100) surfaces are concerned, usually one finds a rotational enhancement smoothly increasing with m[19,42]. We attribute the strong rotational enhancement for $m \geq 1$ found here to the already rather open structure of the (110) surface which leads to a strong corrugation in the H_2-surface interaction (see below). Perpendicular to the troughs which are running along the [10] direction there is a pronounced variation of the barrier position[34]. Then the orientation of the molecule parallel to the surface is not necessarily the energetically most favorable one. This might be the cause for the rotational enhancement of any $m > 0$ rotational mode, not just the $m = j$ helicopter mode.

This strong rotational enhancement has several consequences that could be verified experimentally. As mentioned above, the H_2 molecules in the molecular beam experiments are not in their rovibrational ground state. The distributions are rather characterized by Boltzmann factors with effective temperatures. As far as the rotations are concerned, the corresponding temperature is about 80% of the nozzle temperature T_N, which is related to the kinetic energy[5] by $E_{kin} = \frac{5}{2} k_B T_N$. We have simulated this effect by determining a rotationally averaged sticking probability according to

$$S_{tot}(E_{kin}) = \frac{1}{Z} \sum_{j,m} S(E_{kin}, j, m) \exp\left(\frac{-E_{rot}(j,m)}{k_B T_{rot}}\right) \quad (9)$$

where Z is the partition sum, and T_{rot} is specified by $T_{rot} = 0.8 \cdot T_N = 0.8 \cdot 2E_{kin}/(5k_B)$. The sticking probability determined according to eq. 9 is also included in Fig. 2b. Due to the fact that almost all rotational states with $m > 0$ cause an enhancement of the sticking probability, the combined effect of all rotational states is to lead to an effective increase in the sticking probability at kinetic energies larger than 0.1 eV. This effect should in fact be seen experimentally, if the rotational temperature of the molecular beam is changed by seeding techniques. Please note that the agreement between experiment and theory for $j = 0$ is in fact detoriated when the rotational effects are included in the simulations.

The rotational effects evident in the sticking probabilities should also be observable in the time-reversed process of dissociative adsorption, the associative desorption. According to the principles of microscopic reversibility and detailed balance, the calculated state-resolved sticking probabilties can directly be used to determine the relative populations in desorption[8,17]. The strong rotational enhancement in adsorption should lead to a so-called rotational heating in desorption. The rotational temperature in desorption is related to the mean rotational energy $T_{\mathrm{rot}} = E_{\mathrm{rot}}/k_B$. Thus, the mean rotational energy of desorbing molecules should be larger than in thermal equilibrium. In Fig. 4, we have plotted the calculated rotational temperatures in desorption as a function of the surface temperature. Indeed we find a small rotational heating which, to the best of our knowl-

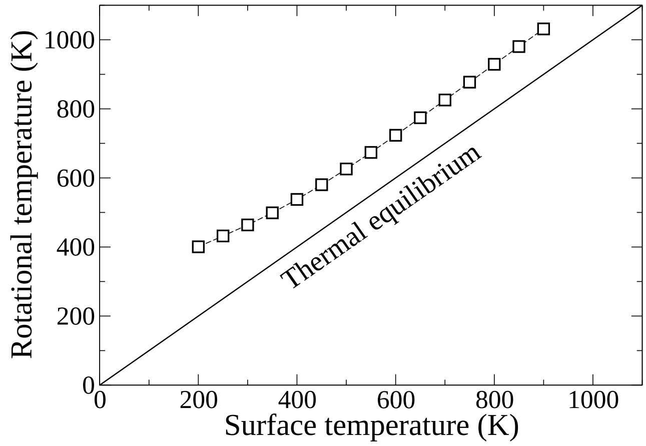

FIG. 4: Rotational temperature of desorbing H_2 molecules as a function of surface temperature. The solid line represents the thermal equilibrium.

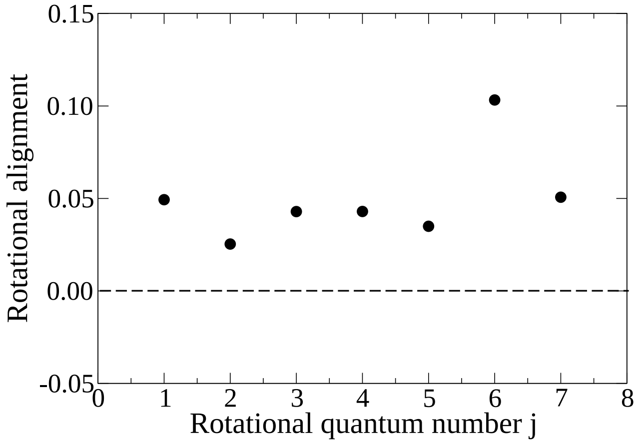

FIG. 5: Calculated rotational alignment in desoprtion as a function of the rotational quantum number for a surface temperature of $T = 700$ K.

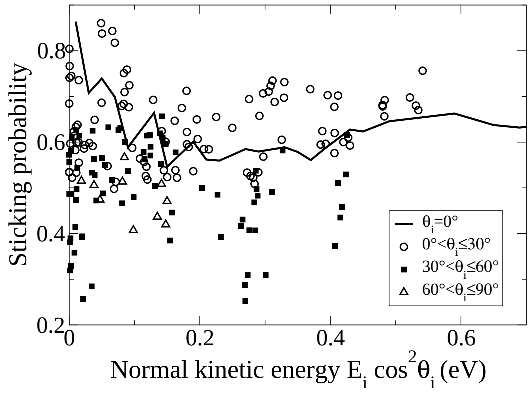

FIG. 6: Sticking probability as a function of normal component of the incident energy for molecules initially in the vibrational and rotational ground state. The solid line denotes the normal-incidence data while the results for non-normal incidence are grouped according to their angle of incidence θ: $0° - 30°$: circles, $30° - 60°$: boxes, $60° - 90°$: triangles. Note that the non-normal incidence data are obtained for different azimuthal angles.

edge, has not been found before in the desorption of molecules. Usally one finds rotational cooling in desorption[8]. Unfortunately, the rotational effects in the system H_2/Pd(110) have not been measured yet. Thus it is very desirable that our prediction will be checked experimentally. We note, however, that for H_2/Pt(110), no rotational enhancement has been found for $j = 1$ and $j = 2$, but rather a rotational hindering[9].

As a further property of desorbing molecules, the rotational alignment can be measured[7,11,43]. It is defined by the quadrupole moment of the orientational distribution of desorbing molecules

$$A_0^{(2)} = \left\langle \frac{3m^2 - j^2}{j^2} \right\rangle . \quad (10)$$

Molecules rotating preferentially in the cartwheel fashion have an alignment parameter $A_0^{(2)}(j) < 0$, while for molecules rotating preferentially in the helicopter fashion $A_0^{(2)}(j) > 0$. From the calculated sticking probabilities, desorption distribution can be directly derived using the principle of microscopic reversibility[8,17]. Fig. 5 shows the calculated rotational alignment for a surface temperature of 700 K. Since the sticking probability is enhanced for $m > 0$, the molecules desorb preferentially in states with $m > 0$. This leads to a positive alignment parameter. However, this alignment is much smaller than found for H_2 and D_2 desorbing from other surfaces[7,17,42–44]. This is at first sight surprising regarding the strong enhancement of the sticking probability for molecules rotating in the helicopter mode. However, all but the $m = 0$ rotational states show a strong enhancement of the sticking probability. The small alignment is caused by the fact that the rotational enhancement is similar for all $m > 0$ states so that there is no pronounced preference for the maximum $m = j$ state.

Let us now focus on the role of the corrugation in the dissociation dynamics. The dependence of the sticking probability on the angle of incidence θ_i is directly related to the corrugation of a surface. For a perfectly smooth surface, the sticking scales with the normal component of the translational energy, i.e., it exhibits the so-called *normal-energy scaling*, while for a corrugated surface also the parallel component of the kinetic energy influences the sticking probability. In Fig. 6, we have summarized our results for the sticking probability for different angles of incidence as a function of the normal component of the kinetic energy. If we had normal-energy scaling, all the data would fall onto the sticking curve for normal incidence, $\theta = 0°$. However, we see that additional parallel momentum strongly influences the sticking probability indicating the strong corrugation of the H_2/Pd(110) PES. The dependence on the angle of incidence is in fact much stronger than on the smoother Pd(100) surface (see Fig. 9 in Ref. 15).

We first note that there is no unique trend in the role of additional parallel momentum. For an angle of incidence larger than 30° the dissociation is surpressed compared to the normal-incidence results. For angles of incidence below 30°, there is both a suppresion and an enhancement of the sticking probability caused by additional parallel momentum. For the majority of incidence conditions with $\theta \leq 30°$, however, additional parallel momentum enhances the dissociation.

Furthermore, we see a large scatter in the data for the same normal kinetic energy. This is caused by the strong corrugation which leads to a strong dependence of the sticking probability on the lateral kinetic energy at the same normal kinetic energy. In addition, it is caused by the azimuthal anisotropy of the (110) surface. The atom rows along the troughs running in the $[1\bar{1}0]$ direction which we denote by [10] or x (see the inset in

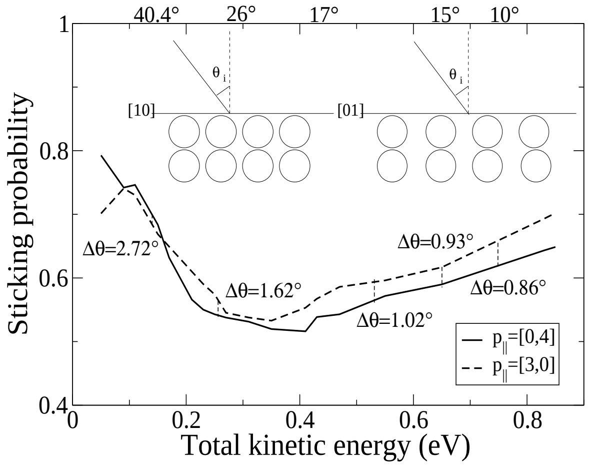

FIG. 7: Sticking probability as a function of the total kinetic energy under non-normal incidence along the [10] and [01] directions, respectively. The parallel momentum has been kept fixed to $p_{\|} = 3\hbar G_X \equiv [30]$ and $p_{\|} = 4\hbar G_Y \equiv [04]$. The corrugation along these different directions is indicated in the insets. The angles of incidence for the [10] direction are shown at the upper axis, and the difference in the incident angles to the [01] direction are added in the figure.

Fig. 1a) are in fact close-packed. One would expect that along this direction the corrugation is relatively weak. However, the DFT calculations[34] showed that there is a strong variation of the barrier height to dissociative adsorption between the top site and the short bridge site along [10], whereas along the [001], [01] or y direction perpendicular to the troughs, it is rather both the barrier position and height that vary.

In Fig. 7, we have plotted the sticking probability for non-normal incidence along the [10] and [01] directions, respectively, for constant parallel momentum. For the sake of computational efficiency, we have determined the sticking probability for non-normal incidence only for parallel momenta that correspond to vectors of the surface reciprocal lattice. Note that the ratio between the length of the two unit vectors of the surface reciprocal lattice is $G_X/G_Y = \sqrt{2}$. Since $\sqrt{2}$ is no rational number, it is impossible to get the same angle of incidence along different azimuths if the parallel momenta are multiples of the reciprocal lattice vectors. In Fig. 7, we show results for two parallel momenta, $p_{\|} = 3\hbar G_X$ and $p_{\|} = 4\hbar G_Y$, since $3G_X \approx 4G_Y$.

We find that except for the lowest energies, the sticking probability for an angle of incidence along the [10] direction is larger than along the [01] direction. However, the differences are still relatively small. We have analysed the dependence of the sticking probability on the angle of incidence for three different azimuths in more detail in Fig. 8. In addition to the [01] and [10] directions we have also considered the [11] direction which corresponds to the diagonal of the surface Brillouin zone. At the lowest kinetic energy, $E_i = 0.05$ eV, the sticking probability is almost independent of the angle of incidence, in agreement with the experiment[39]. A similar behavior has also been found in the case of H_2/Pd(100)[1,15]. At higher kinetic energies, there is first a slight increase in the sticking probabilities with increasing angle of incidence, and then a decrease which is most pronounced at the highest kinetic energy considered, $E_i = 0.7$ eV. Except for the lowest kinetic energies, the highest sticking probabilities are found for the incidence along the [10] direction, which confirms the findings of Fig. 7.

In order to analyse the effect of the corrugation on the sticking probability, it is helpful to distinguish between so-called energetic and geometric corrugation[19,45]. Energetic corrugation corresponds to a situation in which only the barrier height but not its position is varied while in the case of geometric corrugation it is the other way around. In the case of energetic corrugation, additional parallel momentum leads to an effective averaging over the barriers within the surface unit cell. This causes a suppression of the sticking probability for kinetic energies below the average barrier height[19,45]. At a geometrically corrugated surface, on the other hand, the sticking probability is increased by additional parallel momentum. This increase is caused by the fact that an impinging molecular beam under non-normal incidence will hit a larger fraction of barriers where the local potential gradient is aligned to the direction of incidence[19,45]. This effect can be so strong that it leads to an enhanced sticking probability for non-normal incidence for constant kinetic energy. However, it is important to note that for a highly corrugated surface no clear distinction between energetic and geometric corrugation can be made. For example, strong energetic corrugation can lead to a variation of equipotential contour lines below the minimum barrier height that is rather similar to the variation caused by geometric corrugation alone. Furthermore, for a system with both activated and non-activated paths to dissociative adsorption, such as H_2/Pd(110), again no real distinction between energetic and geometric corrugation can be made since for the non-activated paths no barrier location can be defined.

At the lowest kinetic energies in Fig. 8, $E_i = 0.05$ eV, the steering effect is operative. The fact that the sticking probability is almost constant as a function of the polar and azimuthal angle of incidence indicates that the steering effect does not depend on the angle of incidence. At the higher energies, steering becomes less effective. As Fig. 8 shows, the angular dependence of the sticking probability for incident beams along the [10] and the [11] direction are rather similar. Both show first a slight increase as a function of the incident angle with a maximum at 20°-30°, and then a decrease which is the stronger, the higher the kinetic energy.

The [10] direction corresponds to the direction along the close-packed rows of the (110) surface. One would expect that along this direction the corrugation is less pronounced than along the [01] direction which is perpendicular to the troughs of the (110) surface. Hence

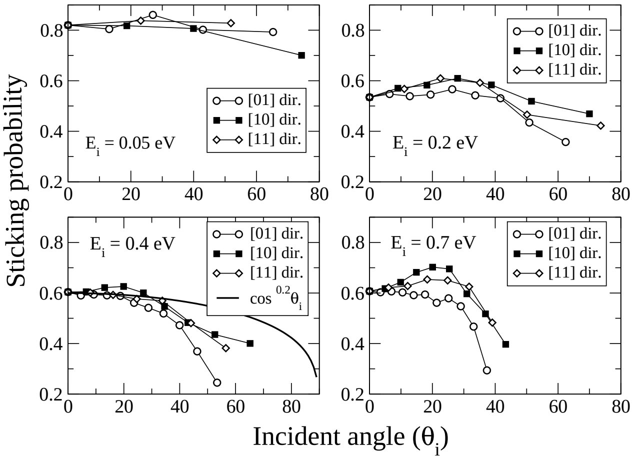

FIG. 8: The sticking probability as a function of incident angle at different initial kinetic energies. The azimuthal angles of incidence are along the [01], [10] and [11] directions, respectively.

it is surprising that we find an initial increase in the sticking probability as a function of the angle of incidence in an energy regime where the sticking probability is rising as a function of kinetic energy for normal incidence. Hence this increase is indicative of a strong corrugation effect along this direction. And indeed, an analysis of the *ab initio* reaction paths listed in Ref. 34 confirms that the variation of the transition state energies for some fixed molecular orientation has a larger variation along the close-packed [10] direction than along the [01] direction (compare, e.g., pathways 4, 5, 6 with pathways 1, 2, 3 or pathways 1 and 8 with pathways 8 and 9 of Ref. 34). Along the [01] direction, i.e. perpendicular to the troughs of the (110) surface, the sticking probability does not exhibit any significant increase as a function of the angle of incidence. This result is in fact in agreement with previous simple three-dimensional calculations for a system with both activated and non-activated paths to dissociative adsorption, where the role of additional parallel momentum has been found to be rather similar to the case of energetic corrugation in a purely activated system[45].

The fact that the results for the azimuthal incidence along [10] and [11] are very similar demonstrates that a molecular beam incident along the diagonal of the surface Brillouin zone also experiences a strong corrugation. In the experiment[39], the incident azimuth has not been specified. For $E_i = 0.35$ eV, the sticking probability has been found to scale according to $S(\theta_i) \propto \cos^{0.2}\theta$. We have included this scaling in the panel for $E_i = 0.4$ eV of Fig. 8. For angles below $30° - 40°$ experiment and theory agree well, depending on the azimuth. Above 40°, the theoretical results seem to be smaller than the experimental curve. However, also the range of incident angles used in the experiment has not been specified in Ref. 39.

IV. CONCLUSIONS

We have performed a quantum dynamical study of the dissociative adsorption and associative desorption of H_2/Pd(110). The potential energy surface has been derived from *ab initio* electronic structure calculations. Our results are in good agreement with the available experimental data. At low kinetic energies, the dissociative adsorption dynamics is dominated by the steering effects due to the coexistence of non-activated and activated paths towards. The open (110) surface is characterized by troughs running along the $[1\bar{1}0]$ direction. The strong corrugation and anisotropy of the potential energy surface lead to pronounced orientational effects in the adsorption and desorption dynamics. We found a strong enhancement of the sticking probability for molecules rotating with azimuthal quantum numbers $m > 0$. This enhancement causes an unusual rotational heating in desorption and a rather small rotational alignment. Due to the strong corrugation, we found a significant deviation from normal-energy scaling in the adsorption at non-normal incidence. For an angle of incidence along the close-packed rows of the Pd(110) surface, we find an initial increase of the sticking probability as a function of the angle of incidence which is indicative of a strong corrugation effect. For an azimuthal incidence perpendicular to the troughs of the Pd(110) surface, there is no signifcant maximum in the sticking probability for non-normal angles of incidence.

[1] K. D. Rendulic, G. Anger, and A. Winkler, Surf. Sci. **208**, 404 (1989).
[2] H. A. Michelsen and D. J. Auerbach, J. Chem. Phys. **94**, 7502 (1991).
[3] C. T. Rettner, D. J. Auerbach, and H. A. Michelsen, Phys. Rev. Lett. **68**, 1164 (1992).
[4] A. Hodgson, J. Moryl, P. Traversaro, and H. Zhao, Nature **356**, 501 (1992).
[5] K. D. Rendulic and A. Winkler, Surf. Sci. **299/300**, 261 (1994).
[6] M. Beutl, M. Riedler, and K. D. Rendulic, Chem. Phys. Lett. **247**, 249 (1995).
[7] D. Wetzig, R. Dopheide, M. Rutkowski, R. David, and H. Zacharias, Phys. Rev. Lett. **76**, 463 (1996).
[8] D. Wetzig, M. Rutkowski, H. Zacharias, and A. Groß, Phys. Rev. B **63**, 205412 (2001).
[9] M. Beutl, M. Riedler, and K. D. Rendulic, Chem. Phys. Lett. **256**, 33 (1996).
[10] M. Gostein and G. O. Sitz, J. Chem. Phys. **106**, 7378 (1997).
[11] H. Hou, S. J. Gulding, C. T. Rettner, A. M. Wodtke, and D. J. Auerbach, Science **277**, 80 (1997).

[12] T. Mitsui, M. K. Rose, E. Fomin, D. F. Ogletree, and M. Salmeron, Nature **422**, 705 (2003).
[13] A. Groß, B. Hammer, M. Scheffler, and W. Brenig, Phys. Rev. Lett. **73**, 3121 (1994).
[14] A. Groß, S. Wilke, and M. Scheffler, Phys. Rev. Lett. **75**, 2718 (1995).
[15] A. Groß and M. Scheffler, Phys. Rev. B **57**, 2493 (1998).
[16] A. Groß and M. Scheffler, Phys. Rev. B **61**, 8425 (2000).
[17] A. Dianat and A. Groß, Phys. Chem. Chem. Phys. **4**, 4126 (2002).
[18] A. Groß, Surf. Sci. Rep. **32**, 291 (1998).
[19] G. R. Darling and S. Holloway, J. Chem. Phys. **101**, 3268 (1994).
[20] G. R. Darling and S. Holloway, Rep. Prog. Phys. **58**, 1595 (1995).
[21] G.-J. Kroes, E. J. Baerends, and R. C. Mowrey, Phys. Rev. Lett. **78**, 3583 (1997).
[22] G.-J. Kroes, Prog. Surf. Sci. **60**, 1 (1999).
[23] G.-J. Kroes, A. Groß, E. J. Baerends, M. Scheffler, and D. A. McCormack, Acc. Chem. Res. **35**, 193 (2002).
[24] A. Eichler, J. Hafner, A. Groß, and M. Scheffler, Phys. Rev. B **59**, 13297 (1999).
[25] W. Diño, H. Kasai, and A. Okiji, Prog. Surf. Sci. **63**, 63 (2000).
[26] Y. Miura, H. Kasai, and W. Diño, J. Phys.: Condens. Matter **14**, L479 (2002).
[27] H. F. Busnengo, W. Dong, and A. Salin, Chem. Phys. Lett. **320**, 328 (2000).
[28] C. Crespos, H. F. Busnengo, W. Dong, and A. Salin, J. Chem. Phys. **114**, 10954 (2001).
[29] H. F. Busnengo, E. Pijper, M. F. Somers, G. J. Kroes, A. Salin, R. A. Olsen, D. Lemoine, and W. Dong, Chem. Phys. Lett. **356**, 515 (2002).
[30] H. F. Di Cesare, M. A. Busnengo, W. Dong, and A. Salin, J. Chem. Phys. **118**, 11226 (2003).
[31] W. Brenig and M. F. Hilf, J. Phys. Condens. Mat. **13**, R61 (2001).
[32] J. N. Murrell, A. T. Yinnon, and R. B. Gerber, Chem. Phys. **33**, 131 (1978).
[33] G.-J. Kroes, J. G. Snijders, and R. C. Mowrey, J. Chem. Phys. **103**, 5121 (1995).
[34] V. Ledentu, W. Dong, and P. Sautet, Surf. Sci. **412**, 518 (1998).
[35] W. Brenig, T. Brunner, A. Groß, and R. Russ, Z. Phys. B **93**, 91 (1993).
[36] W. Brenig and R. Russ, Surf. Sci. **315**, 195 (1994).
[37] S. Wilke and M. Scheffler, Phys. Rev. B **53**, 4926 (1996).
[38] A. Groß and M. Scheffler, Chem. Phys. Lett. **256**, 417 (1996).
[39] C. Resch, H. F. Berger, K. D. Rendulic, and E. Bertel, Surf. Sci. **316**, L1105 (1994).
[40] M. Kay, G. R. Darling, S. Holloway, J. A. White, and D. M. Bird, Chem. Phys. Lett. **245**, 311 (1995).
[41] H. F. Busnengo, A. Salin, and W. Dong, J. Chem. Phys. **112**, 7641 (2000).
[42] A. Groß and M. Scheffler, Prog. Surf. Sci. **53**, 187 (1996).
[43] D. Wetzig, M. Rutkowski, R. Etterich, W. David, and H. Zacharias, Surf. Sci. **402**, 232 (1998).
[44] A. Eichler, J. Hafner, A. Groß, and M. Scheffler, Chem. Phys. Lett. **311**, 1 (1999).
[45] A. Groß, J. Chem. Phys. **102**, 5045 (1995).
[46] V. Ledentu, W. Dong, P. Sautet, A. Eichler, and J. Hafner, Phys. Rev. B **57**, 12482 (1998).